The Title Goes Here with Each Initial Letter Capitalized

Brian L. Frost,[1, a)] C. Elliott Strimbu,[2, b)] and Elizabeth S. Olson[2, 3, c)]

[1)]*Department of Electrical Engineering, Columbia University, 500 W. 120th St., Mudd 1310, New York, New York 10027, USA*
[2)]*Department of Otolaryngology Head and Neck Surgery, Vagelos College of Physicians and Surgeons, Columbia University, 630 W. 168th St., New York, New York 10032, USA*
[3)]*Department of Biomedical Engineering, Columbia University, 351 Engineering Terrace, 1210 Amsterdam Ave., New York, New York 10027, USA*

[a)]*Corresponding author: b.frost@columbia.edu*
[b)]*Electronic mail: ces2243@cumc.columbia.edu*
[c)]*Electronic mail: eao2004@cumc.columbia.edu*

Abstract.

INTRODUCTION

Historically, the in vivo study of cochlear mechanics has been limited to measurements of the basilar membrane (BM). The advent of optical coherence tomography (OCT) in the last decade has allowed for vibrometry at a depth, facilitating the study of intra-organ of Corti complex (OCC) motions. Of particular interest is the motion of the electromotile outer hair cells (OHCs), which play an important role in the amplifying vibration responses and increasing the range of sound-pressure levels (SPLs) over which hearing operates.

Several groups have presented OCT measurements of OHC motion in the base of the sensitive gerbil cochlea. In some instances, these measurements have differed significantly from one another. In particular, groups have reported disparate phase differences between displacements in the “OHC region" and at the BM.

Several aspects complicate these measurements. The first is that the term “OHC region" is ill-defined; the OHCs are 40 μm long and 10 μm wide, and come in rows of three per longitudinal cross-section. Mechanical intuition may lead one to believe that the apical surface of the OHCs, called the reticular lamina (RL), may move differently from the basal surface attached to the Deiters' cells as the OHC compresses and expands due to electromotility. Generally, it is naive to assume that the entire 120 μm^2 OHC region moves uniformly.

A second complication is that measurements are taken at an angle with respect to the orientation of the cochlea, unknown *a priori*. This means that (1) displacements measured via OCT are projections of the three-dimensional motion onto an unknown axis, and (2) measured points at the OHC and BM within a single measurement may lie in different longitudinal cross-sections.

The first of these ambiguities is discussed by Cooper et al (REF), wherein the authors discuss the hypothetical scenario that OHCs exhibit some fluid-like elliptical motions. Their model showed that the phase difference between measured OHC and BM motion relied heavily on the viewing angle, with any deviation between -180 and +180 degrees being achievable. The viewing angle is critical for the assessment of phase differences between OHC and BM motion.

The second of these ambiguities is discussed by Frost et al (REF), wherein we developed a program which measured the relative anatomical displacements between structures measured via OCT. We used this program to account for the longitudinal displacement between measured OHC and BM, and showed that this correction significantly affected the character of OHC phase re BM. This included a discrepancy of up to 90 degrees between displacement-accounted and single-measurement phases at high frequencies.

With these complications in mind, it is difficult to interpret presented OCT measurements of OHC displacement reported without a viewing angle. The group of Ren has achieved RL and OHC displacement measurements (via an interferometer similar to OCT) taken at a purely transverse angle, both in gerbil and mouse (REF). They show that RL phase leads BM at low frequencies, but that this lead decreases monotonically and near-linearly until the structures are in phase at about 80% of the best frequency (BF). After this zero crossing, the RL re BM phase continues its monotonic decrease, with the RL lagging the BM at near- and supra-BF frequencies.

Meanwhile the other hand, our displacement-accounted data (i.e. OHC and BM in the same tonotopic cross-section) taken at a viewing angle with a significant longitudinal component shows a phase difference of a very different character. We see that OHC leads BM across frequency, including at high frequencies – where Ren et al see an 80 degree *lag*, we see a 90 degree *lead*.

We have developed a method to isolate the transverse and longitudinal components of motion of structures within the OCC, wherein we account both for the longitudinal displacement between structures and the projection incurred by the viewing angle. Similar to the work of Lee et al (REF), we do so by taking measurements at multiple viewing angles. Our method requires no *a priori* knowledge of either measurement angle, or of the positions of the structures being measured. We employ a linear approximation of the longitudinal direction at acquisition time, followed by *post hoc* registration of structures measured at several longitudinal locations and viewing angles. We then backproject the measured displacements to achieve a reconstructed longitudinal-transverse profile of a structure's motion.

We present the method, an analysis of its fidelity with respect to viewing angle, as well as *in vivo* data from the base of the gerbil cochlea in which the longitudinal-transverse motion at the base of several OHCs has been reconstructed. In this sample data set, our reconstructed transverse displacements are consistent with previously measured pure-transverse displacements. We also see that longitudinal OHC displacement is generall smaller than transverse OHC displacement in magnitude, and 180 degrees out of phase (with respect to our chose coordinate system) with transverse OHC displacements across frequency.

METHODS

Acquisition

The acquisition process follows a few simple steps: (1) prior to acquisition, ensure the BM looks as horizontal as possible in the orienting B-Scan, (2) determine the approximate longitudinal direction and take measurements of a single structure at multiple longitudinal locations, (3) rotate the preparation and try to isolate similar cross-sections with the BM appearing horizontal in the orienting B-Scan, (4) again, find the approximate longitudinal direction and take measurements of the same structure at multiple longitudinal locations.

Orienting the preparation so that the BM appears horizontal in each cross-section ensures that the radial component of the optic axis is approximately zero. This is important, as we are attempting to simplify our problem to two dimensions – transverse and longitudinal. Failing to account for this radial angle will make our two-dimensional reconstruction impossible.

Determining the approximate longitudinal directions works via a linear approximation of the cochlea's anatomical coordinates, similar to the planar approximation employed in Frost et al, 2022. As we only need the longitudinal direction for acquisition, this is a simpler process – we use ThorImage and locate a landmark in some cross-section; for example, we can choose the base of the OHC, or the thickest part of the BM. We record the optical coordinates at these positions, $p_1 = (x_1, y_1, z_1)$ and $p_2 = x_2, y_2, z_2)$. The difference between these points is a linear approximation of a vector in the longitudinal direction, so the unit longitudinal vector is

$$l = \frac{p_2 - p_1}{|p_2 - p_1|}. \tag{1}$$

We can find points of measurement at fixed increments along the longitudinal direction. If we start at a point q_0, and want to measure N points over longitudinal distance L, we measure at

$$q_n = q_0 + \frac{nL}{N} l,\ n = 0, 1, \ldots, N-1. \tag{2}$$

We take volume scans after each run so that outside of the time pressure of an experiment, we can apply our more complex orientation program (FROST ET AL REF). In doing so, we can assess the accuracy of our assumption that the radial component of our measurement axis is 0, as well as the direction of the longitudinal vector.

Registration

As we have made sure to remove the radial component of motion from our measurements, we can assume the optical z axis is comprised of only longitudinal (l) and transverse (t) components. We write the optical axis' unit vector as a two-dimensional vector in anatomical coordinates, $z = (z_l, z_t)$.

Eqn. 1 is used in the acquisition step to find the longitudinal vector l, which has optical x, y and z components. The z component of this vector represents the amount of longitudinal motion that is projected onto the optical axis, z_l. To find the t component of z, we need only to recall that z is a unit vector, so that $z_l^2 + z_t^2 = 1$. Using the notation from Eqn. 1, we have

$$z_l = \frac{z_2 - z_1}{|p_2 - p_1|}, \tag{3}$$

$$z_t = \sqrt{1 - z_l^2}. \tag{4}$$

Knowing this, we can relate the OHC and BM longitudinal locations within a single measurement. If the structures along a single measurement axis are spaced Δz apart, then the OHCs lie $\Delta l = z_l \Delta z$ apical of the BM. The measured BM Δl apical of this measurement is thereby in the same longitudinal cross-section as the OHC in the first measurement. We call these BM and OHC measurements *aligned* to one another. At each measurement angle, we compose a list of all aligned OHC and BM measurements.

To register points to one another between viewing angles, we use the phase of BM motion. By matching the phase responses of BM measurements taken at different viewing angles, we can register the cross-sections in which these BM motions were measured. This operates under the assumption that BM motion is entirely transverse, so that its phase response at each cross-section will be the same at each viewing angle.

Having registered BM points to one another, we can then consult our list of aligned BM-OHC pairs. The OHCs aligned to registered BM positions are also registered, allowing us to isolate the same OHCs at different viewing angles.

Reconstruction

Each OCT measurement is a projection of a true 3-D motion onto the optical z axis. In the current context, we have made efforts to eliminate the representation of radial motion in our projection,so that the problem can be framed as the projection of a 2-D longitudinal-transverse *true motion* d onto a 2-D transverse-longitudinal z axis, forming the *projected motion* δ.

Above we describe the method by which we determine the z_l and z_t components of the optical axis in each experiment. The projection onto this axis is given by the dot product

$$\delta = z \cdot d = \begin{pmatrix} z_l & z_t \end{pmatrix} \begin{pmatrix} d_l \\ d_t \end{pmatrix}. \tag{5}$$

At each angle, if we are truly measuring at one position, d will remain the same and z will change. If we take measurements at two angles, we form the system of equations:

$$\begin{pmatrix} \delta_1 \\ \delta_2 \end{pmatrix} = \begin{pmatrix} l_1 & t_1 \\ l_2 & t_2 \end{pmatrix} \begin{pmatrix} d_l \\ d_t \end{pmatrix}, \tag{6}$$

where the rows of the matrix are the z axes corresponding to each angle, and δ_i is the projection measured at the i^{th} angle.

We measure δ_i and determine the l and t components of the z axis as described above. We want to reconstruct d, which can be done simply by inverting the matrix in Equation 6. This is possible if and only if the rows of the matrix are linearly independent, i.e. if the measurement axes are not colinear. So long as we measure at two sufficiently distinct (to be quantified shortly) angles, we can reconstruct d by performing the matrix inverse:

$$\begin{pmatrix} d_l \\ d_t \end{pmatrix} = \frac{1}{l_1 t_2 - l_2 t_1} \begin{pmatrix} t_2 & -t_1 \\ -l_2 & l_1 \end{pmatrix} \begin{pmatrix} \delta_1 \\ \delta_2 \end{pmatrix}. \tag{7}$$

Achieving measurements of the same structures at different angles is constrained by the preparation. In practice, a 15 degree rotation is tractable in our preparation, but significantly larger angles are not consistently achievable (yet).

Angular deviation	Condition number κ
20^o	5.67
15^o	7.60
10^o	11.43
5^o	22.90
1^o	114.59

TABLE I. A table of condition numbers for the projection matrix at possible measurement angular deviations.

Of course, one could attempt to reconstruct from measurements taken at angles with only a fraction of a degree of discrepancy, but intuitively this will be unreliable due to the precision of our devices and the noise in the displacement signal.

The precision of our reconstruction can be found via the *condition number* κ of our projection matrix in Equation 6. The condition number is defined as

$$\kappa(A) = \frac{|\sigma_{max}|}{|\sigma_{min}|}, \tag{8}$$

where σ_{max} and σ_{min} are the maximum and minimum singular values of matrix A. The condition number of a matrix represents how “well-posed" a system of equations is, i.e. how close to singular the matrix is. A matrix with a large condition number will amplify noise significantly more than a matrix with a small condition number. The “rule of thumb" is that noise is multiplied by around κ. That is, for $\kappa \approx 10^k$, about k digits of precision are lost via the matrix multiplication. Note that a matrix and its inverse have the same condition number.

Table I shows condition numbers for some possible angular deviations. Condition number does not depend on the absolute angle, but only the absolute difference between the two measurement angles. We should note that our usual precision is on the order of 0.1 nm, and our signal at higher dB SPL is in the range of 1-10 nm.

These should be more-or-less known and kept in mind when analyzing data reconstructed via this method. The realized 15-degree angle will lead to an eight-fold increase in the noise level, which means our results are accurate to about 0.8 nm.

RESULTS

We have employed the method described above in the base of the gerbil cochlea, with measurements taken through the round window membrane at angles of approximately 45^o and 60^o. We take data at 11 positions spaced 15 μm apart longitudinally at each angle, ensuring that at each point we measure a position at the base of the OHCs. We stimulate with one-second, 15-frequency multitone stimuli at 80 dB SPL.

As we step longitudinally along the cochlea, we expect to see the phase response at the BM to vary along with the tonotopic cross-section. This behavior is displayed in Fig. (FIGURE REFERENCE), providing evidence that our acquisition method is truly stepping along the tonotopic axis.

As for the registration process, Fig. (FIGURE REF) shows matched BM phases taken at two different angles. While we did not know the overlap of the measured regions at each angle *a priori*, we have found this 60 μm region of longitudinal overlap *post hoc*. As each of these positions is one longitudinal measurement step apart at their respective angles, this provides evidence that we have correctly taken uniform longitudinal steps at both angles.

Applying our reconstruction method to the associated aligned OHCs we arrive at the two-dimensional frequency responses presented in Fig. (FIGURE REFERENCE). At all registered OHC base locations, we see that transverse OHC motion is significantly larger than longitudinal OHC motion across the bulk of the frequency range at 80 dB. Reconstructed transverse OHC displacement phase undergoes the linear lead-to-lag transition measured by Ren et al (REF), with zero-crossing near 0.8BF.

Interestingly, the longitudinal displacement phase leads transverse displacement phase by about 180 degrees. With respect to our coordinate system, this means that towards-BM transverse displacement is in phase with basal-to-apical longitudinal displacement, with their 2-D transverse-longitudinal displacements being shaped approximately linearly.

CONCLUSION

We have developed and presented the application of a method via which longitudinal-transverse 2-D intra-OCC displacements can be reconstructed from 1-D OCT measurements, without any *a priori* knowledge of the measurement angles or measurement locations. We have presented the application of this method to reconstructing the motion of the base of OHCs across a 45 μm longitudinal region of the base of the cochlea. This method can be used to reconstruct the two-dimensional motion of any structure in the OCC of any animal, so long as the measurement angle can be changed by a sufficient amount.

A 2-D understanding of intra-OCC motions provides significantly more information about the mechanical operations of structures within, including power transfer of OHCs to the BM. Measurements of this type help to resolve discrepancies between groups, contextualize 1-D measurements and serve as a step towards the goal of reconstructing total 3-D intra-OCC displacements.

FIRST-LEVEL HEADING: THE LINE BREAK WAS FORCED via \\

This sample document demonstrates proper use of REVTEX 4.1 (and LATEX 2_ε) in manuscripts prepared for submission to AIP conference proceedings. Further information can be found in the documentation included in the distribution or available at `http://authors.aip.org` and in the documentation for REVTEX 4.1 itself.

When commands are referred to in this example file, they are always shown with their required arguments, using normal TEX format. Ithis format, `#1`, `#2`, etc. stand for required author-supplied arguments to commands. For example, in `\section{#1}` the `#1` stands for the title text of the author's section heading, and in `\title{#1}` the `#1` stands for the title text of the paper.

Line breaks in section headings at all levels can be introduced using \\. A blank input line tells TEX that the paragraph has ended.

Second-level heading: Formatting

This file may be formatted in both the `preprint` (the default) and `reprint` styles; the latter format may be used to mimic final journal output. Either format may be used for submission purposes. Hence, it is essential that authors check that their manuscripts format acceptably under `preprint`. Manuscripts submitted to AIP that do not format correctly under the `preprint` option may be delayed in both the editorial and production processes.

Third-level heading: Citations and Footnotes

Citations in text refer to entries in the Bibliography; they use the commands `\cite{#1}` or `\onlinecite{#1}`. Because REVTEX uses the `natbib` package of Patrick Daly, its entire repertoire of commands are available in your document; see the `natbib` documentation for further details. The argument of `\cite` is a comma-separated list of *keys*; a key may consist of letters and numerals.

By default, citations are numerical; [1] author-year citations are an option. To give a textual citation, use `\onlinecite{#1}`: (Refs. 2, 3, and 4). REVTEX "collapses" lists of consecutive numerical citations when appropriate. REVTEX provides the ability to properly punctuate textual citations in author-year style; this facility works correctly with numerical citations only with `natbib`'s compress option turned off. To illustrate, we cite several together [1, 2, 3, 5], and once again (Refs. 1, 3, 4, and 5). Note that, when numerical citations are used, the references were sorted into the same order they appear in the bibliography.

A reference within the bibliography is specified with a `\bibitem{#1}` command, where the argument is the citation key mentioned above. `\bibitem{#1}` commands may be crafted by hand or, preferably, generated by using BibTEX. The AIP styles for REVTEX 4 include BibTEX style files `aipnum.bst` and `aipauth.bst`, appropriate for numbered and author-year bibliographies, respectively. REVTEX 4 will automatically choose the style appropriate for the document's selected class options: the default is numerical, and you obtain the author-year style by specifying a class option of `author-year`.

This sample file demonstrates a simple use of the BibTEX tool via a `\bibliography` command referencing the `aipsamp.bib` file. Running BibTEX (in this case `bibtex aipsamp`) after the first pass of LATEX produces the file `aipsamp.bbl` which contains the automatically formatted `\bibitem` commands (including extra markup information via `\bibinfo` commands). If not using BibTEX, the `thebibiliography` environment should be used instead.

Fourth-level heading is run in. Footnotes are produced using the `\footnote{#1}` command. Numerical style citations put footnotes into the bibliography [6]. Author-year and numerical author-year citation styles (each for its own reason) cannot use this method. Note: due to the method used to place footnotes in the bibliography, *you must re-run BibTeX every time you change any of your document's footnotes*.

MATH AND EQUATIONS

Inline math may be typeset using the `$` delimiters. Bold math symbols may be achieved using the `bm` package and the `\bm{#1}` command it supplies. For instance, a bold α can be typeset as `$\bm{\alpha}$` giving $\boldsymbol{\alpha}$. Fraktur and Blackboard (or open face or double struck) characters should be typeset using the `\mathfrak{#1}` and `\mathbb{#1}` commands respectively. Both are supplied by the `amssymb` package. For example, `$\mathbb{R}$` gives $\mathbb{R}$ and `$\mathfrak{G}$` gives $\mathfrak{G}$

In LATEX there are many different ways to display equations, and a few preferred ways are noted below. Displayed math will center by default. Use the class option `fleqn` to flush equations left.

Below we have numbered single-line equations, the most common kind:

$$\chi_{+}(p) \lesssim [2|\mathbf{p}|(|\mathbf{p}|+p_z)]^{-1/2} \begin{pmatrix} |\mathbf{p}|+p_z \\ px+ip_y \end{pmatrix}, \tag{9}$$

$$\left\{ 1\!\!1234567890abc123\alpha\beta\gamma\delta1234556\alpha\beta\frac{1\sum_b^a}{A^2} \right\}. \tag{10}$$

Note the open one in Eq. (10).

Not all numbered equations will fit within the text width this way. The equation number will move down automatically if it cannot fit on the same line with a one-line equation:

$$\left\{ ab12345678abc123456abcdef\alpha\beta\gamma\delta1234556\alpha\beta\frac{1\sum_b^a}{A^2} \right\} (1234567890abcdefghijklmnopqrstuvwxyz123456789). \tag{11}$$

When the `\label{#1}` command is used [cf. input for Eq. (10)], the equation can be referred to in text without knowing the equation number that TEX will assign to it. Just use `\ref{#1}`, where `#1` is the same name that used in the `\label{#1}` command.

Unnumbered single-line equations can be typeset using the `\[`, `\]` format:

$$g^+g^+ \to g^+g^+g^+g^+\ldots\,,\quad q^+q^+ \to q^+g^+g^+\ldots\,.$$

Multiline equations

Multiline equations are obtained by using the `eqnarray` environment. Use the `\nonumber` command at the end of each line to avoid assigning a number:

$$\begin{aligned} \mathscr{M} =& ig_Z^2(4E_1E_2)^{1/2}(l_i^2)^{-1}\delta_{\sigma_1,-\sigma_2}(g_{\sigma_2}^e)^2\chi_{-\sigma_2}(p_2) \\ & \times[\varepsilon_j l_i \varepsilon_i]_{\sigma_1}\chi_{\sigma_1}(p_1), \end{aligned} \tag{12}$$

$$\begin{aligned} \sum|M_g^{\text{viol}}|^2 =& \, g_S^{2n-4}(Q^2)\, N^{n-2}(N^2-1) \\ & \times\left(\sum_{i<j}\right)\sum_{\text{perm}}\frac{1}{S_{12}}\frac{1}{S_{12}}\sum_\tau c_\tau^f\,. \end{aligned} \tag{13}$$

Note: Do not use `\label{#1}` on a line of a multiline equation if `\nonumber` is also used on that line. Incorrect cross-referencing will result. Notice the use `\text{#1}` for using a Roman font within a math environment.

TABLE II. This table illustrates left-aligned, centered, and right-aligned columns. Note that REVTEX 4 adjusts the intercolumn spacing so that the table fills the entire width of the text. Table captions are numbered automatically.

Left[a]	Centered[b]	Right
1	2	3
10	20	30
100	200	300

[a] Note a.
[b] Note b.

To set a multiline equation without *any* equation numbers, use the `\begin{eqnarray*}`, `\end{eqnarray*}` format:

$$\sum |M_g^{\rm viol}|^2 = g_S^{2n-4}(Q^2)\, N^{n-2}(N^2-1) \times \left(\sum_{i<j}\right)\left(\sum_{\rm perm}\frac{1}{S_{12}S_{23}S_{n1}}\right)\frac{1}{S_{12}}\,.$$

To obtain numbers not normally produced by the automatic numbering, use the `\tag{#1}` command, where `#1` is the desired equation number. For example, to get an equation number of (5.1′),

$$g^+g^+ \to g^+g^+g^+g^+\ldots\,,\quad q^+q^+ \to q^+g^+g^+\ldots\,. \tag{5.1′}$$

A few notes on `\tag{#1}`. `\tag{#1}` requires `amsmath`. The `\tag{#1}` must come before the `\label{#1}`, if any. The numbering set with `\tag{#1}` is *transparent* to the automatic numbering in REVTEX; therefore, the number must be known ahead of time, and it must be manually adjusted if other equations are added. `\tag{#1}` works with both single-line and multiline equations. `\tag{#1}` should only be used in exceptional case - do not use it to number all equations in a paper.

Enclosing single-line and multiline equations in `\begin{subequations}` and `\end{subequations}` will produce a set of equations that are "numbered" with letters, as shown in Eqs. (14a) and (14b) below:

$$\left\{abc123456abcdef\alpha\beta\gamma\delta1234556\alpha\beta\frac{1\sum_b^a}{A^2}\right\}, \tag{14a}$$

$$\begin{aligned}\mathscr{M} =& ig_Z^2(4E_1E_2)^{1/2}(l_i^2)^{-1}(g_{\sigma_2}^e)^2\chi_{-\sigma_2}(p_2)\\ &\times[\varepsilon_i]_{\sigma_1}\chi_{\sigma_1}(p_1).\end{aligned} \tag{14b}$$

Putting a `\label{#1}` command right after the `\begin{subequations}`, allows one to reference all the equations in a subequations environment. For example, the equations in the preceding subequations environment were Eqs. (14).

CROSS-REFERENCING

REVTEX will automatically number sections, equations, figure captions, and tables. In order to reference them in text, use the `\label{#1}` and `\ref{#1}` commands. To reference a particular page, use the `\pageref{#1}` command.

The `\label{#1}` should appear in a section heading, within an equation, or in a table or figure caption. The `\ref{#1}` command is used in the text where the citation is to be displayed. Some examples: Section on page 5, Table II, and Fig. 1.

FIGURES AND TABLES

Figures and tables are typically "floats"; LATEX determines their final position via placement rules. LATEX isn't always successful in automatically placing floats where you wish them.

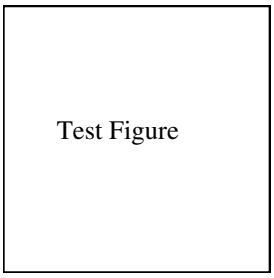

FIGURE 1. A figure caption. The figure captions are automatically numbered.

TABLE III. Numbers in columns Three–Five have been aligned by using the "d" column specifier (requires the `dcolumn` package). Non-numeric entries (those entries without a ".") in a "d" column are aligned on the decimal point. Use the "D" specifier for more complex layouts.

One	Two	Three	Four	Five
one	two	three	four	five
He	2	2.77234	45672.	0.69
C[a]	C[b]	12537.64	37.66345	86.37

[a] Some tables require footnotes.
[b] Some tables need more than one footnote.

Figures are marked up with the `figure` environment, the content of which imports the image (`\includegraphics`) followed by the figure caption (`\caption`). The argument of the latter command should itself contain a `\label` command if you wish to refer to your figure with `\ref`.

Import your image using either the `graphics` or `graphicx` packages. Both of these packages define the `\includegraphics{#1}` command, but they differ in the optional arguments for specifying the orientation, scaling, and translation of the figure. Fig. 1 is an example of this.

The analog of the `figure` environment is `table`, which uses the same `\caption` command. However, you should type your caption command first within the `table`, instead of last as you did for `figure`.

The heart of any table is the `tabular` environment, which represents the table content as a (vertical) sequence of table rows, each containing a (horizontal) sequence of table cells. Cells are separated by the `&` character; the row terminates with `\\`. The required argument for the `tabular` environment specifies how data are displayed in each of the columns. For instance, a column may be centered (`c`), left-justified (`l`), right-justified (`r`), or aligned on a decimal point (`d`). (Table III illustrates the use of decimal column alignment.)

Extra column-spacing may be be specified as well, although REVTEX 4 sets this spacing so that the columns fill the width of the table. Horizontal rules are typeset using the `\hline` command. The doubled (or Scotch) rules that appear at the top and bottom of a table can be achieved by enclosing the `tabular` environment within a `ruledtabular` environment. Rows whose columns span multiple columns can be typeset using LATEX's `\multicolumn{#1}{#2}{#3}` command (for example, see the first row of Table IV).

TABLE IV. This table demonstrates the use of `\multicolumn` in rows with entries that span more than one column.

	D_{4h}^{1}		D_{4h}^{5}	
Ion	1st alternative	2nd alternative	lst alternative	2nd alternative
K	$(2e)+(2f)$	$(4i)$	$(2c)+(2d)$	$(4f)$
Mn	$(2g)$[a]	$(a)+(b)+(c)+(d)$	$(4e)$	$(2a)+(2b)$
Cl	$(a)+(b)+(c)+(d)$	$(2g)$[b]	$(4e)$[a]	
He	$(8r)$[a]	$(4j)$[a]	$(4g)$[a]	
Ag		$(4k)$[a]		$(4h)$[a]

[a] The z parameter of these positions is $z \sim \frac{1}{4}$.
[b] This is a footnote in a table. It is supposed to set on the full width of the page, just as the caption does.

TABLE V. A table with more columns still fits properly in a column. Note that several entries share the same footnote. Inspect the LaTeX input for this table to see exactly how it is done.

	r_c (Å)	r_0 (Å)	κr_0		r_c (Å)	r_0 (Å)	κr_0
Cu	0.800	14.10	2.550	Sn[a]	0.680	1.870	3.700
Ag	0.990	15.90	2.710	Pb[b]	0.450	1.930	3.760
Au	1.150	15.90	2.710	Ca[c]	0.750	2.170	3.560
Mg	0.490	17.60	3.200	Sr[d]	0.900	2.370	3.720
Zn	0.300	15.20	2.970	Li[b]	0.380	1.730	2.830
Cd	0.530	17.10	3.160	Na[e]	0.760	2.110	3.120
Hg	0.550	17.80	3.220	K[e]	1.120	2.620	3.480
Al	0.230	15.80	3.240	Rb[c]	1.330	2.800	3.590
Ga	0.310	16.70	3.330	Cs[d]	1.420	3.030	3.740
In	0.460	18.40	3.500	Ba[e]	0.960	2.460	3.780
Tl	0.480	18.90	3.550				

[a] Here's the first, from Ref. 1.
[b] Here's the second.
[c] Here's the third.
[d] Here's the fourth.
[e] And etc.

TABLE VI. First narrow table.

Element Symbol	Element Name
H	Hydrogen

TABLE VII. Second narrow table, set alongside.

Trial	Time (s)
1	2.42
2	2.46
3	2.41

TABLE VIII. Third narrow table, set alongside once again.

Case	Result
A	Pass
B	Fail
C	Pass

The tables in this document illustrate various effects. Lengthy tables may need to break across pages. A simple way to allow this is to specify the `[H]` float placement on the `table` environment. Alternatively, using the standard LaTeX 2_ε package `longtable` gives more control over how tables break and allows headers and footers to be specified for each page of the table. An example of the use of `longtable` can be found in the file `summary.tex` that is included with the REVTeX 4 distribution.

There are two methods for setting footnotes within a table (these footnotes will be displayed directly below the table rather than at the bottom of the page or in the bibliography). The easiest and preferred method is just to use the `\footnote{#1}` command. This will automatically enumerate the footnotes with lowercase roman letters. However, it is sometimes necessary to have multiple entries in the table share the same footnote. In this case, create the footnotes using `\footnotemark[#1]` and `\footnotetext[#1]{#2}`. `#1` is a numeric value. Each time the same value for `#1` is used, the same mark is produced in the table. The `\footnotetext[#1]{#2}` commands are placed after the `tabular` environment. Examine the LaTeX source and output for Tables II and V for an illustration.

Sometimes it can be convenient to place multiple narrow figures or tables side-by-side to conserve space and meet any page length requirements for your conference. This can be done using `minipage` environments within the `table` or `figure` environment. Check the LaTeX source and output for Tables VI, VII, and VIII for an example of how to do this. The vertical alignment of the `minipage`s can be adjusted by changing the optional argument to the environment.

All AIP journals require that the initial citation of figures or tables be in numerical order. LaTeX's automatic numbering of floats is your friend here: just put each `figure` environment immediately following its first reference (`\ref`), as we have done in this example file.

CONCLUSION

In this section we welcome you to include a summary of the end results of your research.

ACKNOWLEDGMENTS

We wish to acknowledge the support of the author community in using REVTEX, offering suggestions and encouragement, testing new versions, ...

REFERENCES

1. R. P. Feynman, Phys. Rev. **94**, 262 (1954).
2. E. Witten, (2001), hep-th/0106109.
3. A. Einstein, Yu. Podolsky, and N. Rosen, Phys. Rev. **47**, 777 (1935).
4. N. D. Birell and P. C. W. Davies, *Quantum Fields in Curved Space* (Cambridge University Press, 1982).
5. G. P. Berman, Jr. and F. M. Izrailev, Jr., "Stability of nonlinear modes," Physica D **88**, 445 (1983).
6. Automatically placing footnotes into the bibliography requires using BibTeX to compile the bibliography.
7. E. B. Davies and L. Parns, "Trapped modes in acoustic waveguides," Q. J. Mech. Appl. Math. **51**, 477–492 (1988).
8. E. Beutler, "Williams hematology," (McGraw-Hill, New York, 1994) Chap. 7, pp. 654–662, 5th ed.
9. D. E. Knuth, "Fundamental algorithms," (Addison-Wesley, Reading, Massachusetts, 1973) Section 1.2, pp. 10–119, 2nd ed., a full INBOOK entry.
10. J. S. Smith and G. W. Johnson, Philos. Trans. R. Soc. London, Ser. B **777**, 1395 (2005).
11. W. J. Smith, T. J. Johnson, and B. G. Miller, "Surface chemistry and preferential crystal orientation on a silicon surface," J. Appl. Phys. (unpublished).
12. V. K. Smith, K. Johnson, and M. O. Klein, "Surface chemistry and preferential crystal orientation on a silicon surface," J. Appl. Phys. (submitted).
13. U. Ünderwood, N. Ñet, and P. P̄ot, "Lower bounds for wishful research results," (1988), talk at Fanstord University (A full UNPUBLISHED entry).
14. M. P. Johnson, K. L. Miller, and K. Smith, personal communication (2007).
15. J. Smith, ed., *AIP Conf. Proc.*, Vol. 841 (2007).
16. W. V. Oz and M. Yannakakis, eds., *Proc. Fifteenth Annual*, All ACM Conferences No. 17, ACM (Academic Press, Boston, 1983) a full PROCEEDINGS entry.
17. Y. Burstyn, "Proceedings of the 5th International Molecular Beam Epitaxy Conference, Santa Fe, NM," (2004), (unpublished).
18. B. Quinn, ed., *Proceedings of the 2003 Particle Accelerator Conference, Portland, OR, 12-16 May 2005* (Wiley, New York, 2001) albeit the conference was held in 2005, it was the 2003 conference, and the proceedings were published in 2001; go figure.
19. A. G. Agarwal, "Proceedings of the Fifth Low Temperature Conference, Madison, WI, 1999," Semiconductors **66**, 1238 (2001).
20. R. Smith, "Hummingbirds are our friends," J. Appl. Phys. (these proceedings) Abstract No. DA-01.
21. J. Smith, Proc. SPIE **124**, 367 (2007), required title is missing.
22. T. Térrific, "An $O(n \log n / \log \log n)$ sorting algorithm," Wishful Research Result 7 (Fanstord University, Computer Science Department, Fanstord, California, 1988) a full TECHREPORT entry.
23. J. Nelson, TWI Report 666/1999 (Jan. 1999) required institution missing.
24. W. K. Fields, ECE Report No. AL944 (2005) required institution missing.
25. Y. M. Zalkins, e-print arXiv:cond-mat/040426 (2008).
26. J. Nelson, U.S. Patent No. 5,693,000 (12 Dec. 2005).
27. J. K. Nelson, M.S. thesis, New York University (1999).
28. É. Masterly, *Mastering Thesis Writing*, Master's project, Stanford University, English Department (1988), a full MASTERSTHESIS entry.
29. S. M. Smith, Ph.D. thesis, Massachusetts Institute of Technology (2003).
30. S. R. Kawa and S.-J. Lin, J. Geophys. Res. **108**, 4201 (2003), DOI:10.1029/2002JD002268.
31. F. P. Phony-Baloney, *Fighting Fire with Fire: Festooning French Phrases*, PhD dissertation, Fanstord University, Department of French (1988), a full PHDTHESIS entry.
32. D. E. Knuth, *Seminumerical Algorithms*, 2nd ed., The Art of Computer Programming, Vol. 2 (Addison-Wesley, Reading, Massachusetts, 1981) a full BOOK entry.
33. J. C. Knvth, "The programming of computer art," Vernier Art Center, Stanford, California (1988), a full BOOKLET entry.
34. R. Ballagh and C. Savage, "Bose-einstein condensation: from atomic physics to quantum fluids, proceedings of the 13th physics summer school," (World Scientific, Singapore, 2000) cond-mat/0008070.
35. W. Opechowski and R. Guccione, "Introduction to the theory of normal metals," in *Magnetism*, Vol. IIa, edited by G. T. Rado and H. Suhl (Academic Press, New York) p. 105.
36. W. Opechowski and R. Guccione, "Introduction to the theory of normal metals," in *Magnetism*, Vol. IIa, edited by G. T. Rado and H. Suhl (Academic Press, New York, 1965) p. 105.
37. J. M. Smith, "Molecular dynamics," (Academic, New York, 1980).
38. V. E. Zakharov and A. B. Shabat, "Exact theory of two-dimensional self-focusing and one-dimensional self-modulation of waves in nonlinear media," Zh. Eksp. Teor. Fiz. **61**, 118–134 (1971), [Sov. Phys. JETP **34**, 62 (1972)].
39. E. Beutler, in *Williams Hematology*, Vol. 2, edited by E. Beutler, M. A. Lichtman, B. W. Coller, and T. S. Kipps (McGraw-Hill, New York, 1994) 5th ed., Chap. 7, pp. 654–662.
40. R. Ballagh and C. Savage, "Bose-einstein condensation: from atomic physics to quantum fluids," in *Proceedings of the 13th Physics Summer School*, edited by C. Savage and M. Das (World Scientific, Singapore, 2000) cond-mat/0008070.
41. W. Opechowski and R. Guccione, "Introduction to the theory of normal metals," in *Magnetism*, Vol. IIa, edited by G. T. Rado and H. Suhl (Academic Press, New York, 1965) p. 105.

42. J. M. Smith, in *Molecular Dynamics*, edited by C. Brown (Academic, New York, 1980).
43. D. D. Lincoll, "Semigroups of recurrences," in *High Speed Computer and Algorithm Organization*, Fast Computers No. 23, edited by D. J. Lipcoll, D. H. Lawrie, and A. H. Sameh (Academic Press, New York, 1977) 3rd ed., Part 3, pp. 179–183, a full INCOLLECTION entry.
44. A. V. Oaho, J. D. Ullman, and M. Yannakakis, "On notions of information transfer in VLSI circuits," in *Proc. Fifteenth Annual ACM*, All ACM Conferences No. 17, edited by W. V. Oz and M. Yannakakis, ACM (Academic Press, Boston, 1983) pp. 133–139, a full INPROCEDINGS entry.
45. L. Manmaker, *The Definitive Computer Manual*, Chips-R-Us, Silicon Valley, silver ed. (1986), a full MANUAL entry.